Article

General, Room-Temperature Method for the Synthesis of Isolated as Well as Arrays of Single-Crystalline ABO-Type Nanorods

Yuanbing Mao, and Stanislaus S. Wong

J. Am. Chem. Soc., **2004**, 126 (46), 15245-15252• DOI: 10.1021/ja046331j • Publication Date (Web): 02 November 2004

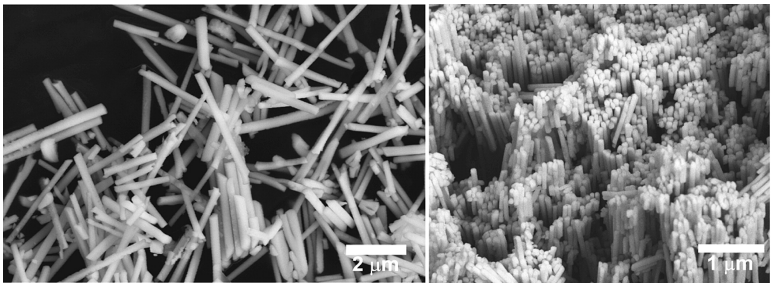

J|A|C|S
ARTICLES
Published on Web 11/02/2004

General, Room-Temperature Method for the Synthesis of Isolated as Well as Arrays of Single-Crystalline ABO_4-Type Nanorods

Yuanbing Mao[†] and Stanislaus S. Wong*[,†,‡]

Contribution from the Department of Chemistry, State University of New York at Stony Brook, Stony Brook, New York 11794-3400, and Materials and Chemical Sciences Department, Brookhaven National Laboratory, Building 480, Upton, New York 11973

Received June 21, 2004; E-mail: sswong@notes.cc.sunysb.edu; sswong@bnl.gov

Abstract: Single-crystalline $BaWO_4$ and $BaCrO_4$ nanorods of reproducible shape and of varying sizes have been controllably prepared using a simple, room-temperature approach, based on the use of porous alumina template membranes. Aligned $BaWO_4$ and $BaCrO_4$ nanorod arrays can be obtained by dissolving the template. Our facile technique, which is analogous to biomineralization, offers a promising and generalized methodology to prepare other types of free-standing ABO_4 nanorods and their corresponding nanorod arrays. Extensive characterization of these samples has been performed using scanning electron microscopy (SEM), transmission electron microscopy (TEM), high-resolution transmission electron microscopy (HRTEM), energy-dispersive X-ray spectroscopy (EDS), selected area electron diffraction (SAED), Raman spectroscopy, FT-infrared spectroscopy (FT-IR), and X-ray diffraction (XRD).

Introduction

Nanoscale structures, such as nanoparticles, nanorods, nanowires, nanocubes, and nanotubes, have attracted extensive synthetic attention as a result of their novel size-dependent properties.[1−7] In particular, one-dimensional (1-D) materials with their inherent anisotropy are the smallest dimension structures that can be used for efficient transport of electrons and optical excitations. As such, they are applicable as building blocks to assemble the next generation of molecular electronic and computational devices. Part of the challenge of developing practical nanoscale devices for a variety of applications, including energy storage, fuel cells, and sensing, is the ability to conveniently synthesize well-characterizable, single-crystalline nanostructures in order to rationally exploit their nanoscale optical, electronic, thermal, and mechanical properties.[6,8−10] Ideally, the net result of nanoscale synthesis is the production of structures that achieve monodispersity, stability, and crystallinity with a predictable morphology. Many of the synthetic methods used to attain these goals have been based on principles derived from semiconductor technology, solid-state chemistry, and molecular inorganic cluster chemistry.

Strategies for the preparation of 1-D nanowires, for example, rely on the formation from a confined alloy droplet, as described by the vapor−liquid−solid (VLS) mechanism,[3,11] the kinetic control of growth through the use of capping reagents,[12,13] the generation through a low temperature, *chimie douce* solution chemical methodology,[14,15] and the use of template-inspired methodologies.[16,17] Metal oxides, in particular, represent one of the most diverse classes of materials, with important structure-related properties, including superconductivity, ferroelectricity, magnetism, conductivity, and gas sensing capabilities.[18,19] It is evident that these types of 1-D oxide nanostructures will lead to key applications in electronics and in the construction of the next generation of electronic and computational devices. Considerable research efforts have been undertaken to synthesize single-crystalline nanomaterials with high purity in large quantities.[1,20,21] However, there are still no generalizable guidelines for their straightforward synthesis with specific chemical and

[†] Department of Chemistry, State University of New York at Stony Brook.

[‡] Materials and Chemical Sciences Department, Brookhaven National Laboratory.

(1) Xia, Y.; Yang, P.; Sun, Y.; Wu, Y.; Mayers, B.; Gates, B.; Yin, Y.; Kim, F.; Yan, H. *Adv. Mater.* **2003**, *15*, 353.
(2) Patzke, G. R.; Krumeich, F.; Nesper, R. *Angew. Chem., Int. Ed.* **2002**, *41*, 2446.
(3) Wu, Y.; Yan, H.; Huang, M.; Messer, B.; Song, J. H.; Yang, P. *Chem. Eur. J.* **2002**, *8*, 1260.
(4) Tremel, W. *Angew. Chem., Int. Ed.* **1999**, *38*, 2175.
(5) Tenne, R. *Chem. Eur. J.* **2002**, *8*, 5296.
(6) Rao, C. N. R.; Cheetham, A. K. *J. Mater. Chem.* **2001**, *11*, 2887.
(7) Rao, C. N. R.; Nath, M. *J. Chem. Soc., Dalton Trans.* **2003**, *(1)*, 1.
(8) Duan, X.; Huang, Y.; Cui, Y.; Wang, J.; Lieber, C. M. *Nature* **2001**, *409*, 66.
(9) Rueckes, T.; Kim, K.; Joselevich, E.; Tseng, G. Y.; Cheung, C.-L.; Lieber, C. M. *Science* **2000**, *289*, 94.
(10) Gao, Y.; Bando, Y. *Nature* **2002**, *415*, 599.
(11) Hu, J.; Odom, T. W.; Lieber, C. M. *Acc. Chem. Res.* **1999**, *32*, 435.
(12) Peng, Z. A.; Peng, X. *J. Am. Chem. Soc.* **2002**, *124*, 3343.
(13) Puntes, V. F.; Krishnan, K. M.; Alivisatos, A. P. *Science* **2001**, *291*, 2115.
(14) Song, J. H.; Messer, B.; Wu, Y.; Kind, H.; Yang, P. *J. Am. Chem. Soc.* **2001**, *123*, 9714.
(15) Mo, M.; Zeng, J.; Liu, X.; Yu, W.; Zhang, S.; Qian, Y. *Adv. Mater.* **2002**, *14*, 1658.
(16) Limmer, S. J.; Seraji, S.; Forbess, M. J.; Wu, Y.; Chou, T. P.; Nguyen, C.; Cao, G. Z. *Adv. Mater.* **2001**, *13*, 1269.
(17) Ginzburg-Margau, M.; Fournier-Bidoz, S.; Coombs, N.; Ozin, G. A.; Manners, I. *Chem. Commun.* **2002**, *(24)*, 3022.
(18) Smart, L.; Moore, E. *Solid State Chemistry*, 2nd ed.; Chapman & Hall: New York, 1995.
(19) West, A. R. *Basic Solid State Chemistry*, 2nd ed.; John Wiley & Sons: New York, 1999.
(20) Mao, Y.; Banerjee, S.; Wong, S. S. *Chem. Commun.* **2003**, *(3)*, 408.
(21) Mao, Y.; Banerjee, S.; Wong, S. S. *J. Am. Chem. Soc.* **2003**, *125*, 15718.

10.1021/ja046331j CCC: $27.50

morphological composition as well as tailor-made sizes and aspect ratios.[1,20,21]

Whereas oxide nanostructures have been synthesized by heating and calcination of precursors,[7] reversed micelle templating techniques,[22,23] sol−gel processes,[24] surfactant-mediated steps,[25] and hydrothermal procedures,[26] in this manuscript, we have relied on a modified template synthesis,[27−29] a relatively simple and versatile method to prepare size-controlled nanostructures.[30] This methodology involves the synthesis of the desired material within the pores of template membranes. The chemical and physical properties of these membranes (i.e., pore geometry and monodisperse diameters) enable a high degree of control over the dimensions of the resulting 1-D nanostructures. Another useful feature of this technique is that it is extremely generalizable with respect to the types of materials that can be synthesized. Indeed, nanotubes and nanofibrils of conductive polymers, metals, semiconductors, carbon, and other types of materials have been prepared within the confined cylindrical pores of membranes.[31−33] Moreover, these tubular or fibrillar nanostructures can be assembled into a wide variety of different architectures. For instance, if a nanostructure-containing membrane is attached to a substrate and the membrane is removed, an ordered assembly of micro- or nanostructures, protruding out from the surface of the substrate, can be obtained, as we have demonstrated in this work.

Though many types of templates exist for the synthesis of 1-D nanostructures, porous anodic alumina membranes are an ideal choice for templating because of their high pore density, parallel and straight channels, distribution of cylindrical pores of highly uniform diameter arranged in a hexagonal array, and size tunability of ca. 5 to 300 nm. Moreover, these templates are thermally and mechanically stable, with readily achievable pore densities as high as 10^{11} pores/cm^2.[31−33]

In this manuscript, we have chosen to focus on the fabrication of nanorods of $BaWO_4$ and $BaCrO_4$, which are compositionally and structurally representative of the ABO_4 class of metal oxides, where A and B are two different metallic elements with oxidation states of +2 and +6, respectively.[34,35] Barium tungstate, $BaWO_4$ (also called Barite), for instance, is important in the electrooptical industry due to its emission of blue luminescence, ascribed to the influence of the Jahn−Teller effect on the degenerated excited state of the $(WO_4)^{2-}$ tetrahedral structure. In addition, its interesting thermoluminescence and stimulated Raman scattering (SRS) properties render barium tungstate as a candidate for the design of solid-state lasers that can emit radiation within a specific spectral region. As such, these materials are of use for medical laser treatment applications, up-conversion fiber lasers, and analogous spectroscopic functions.[36−38] Barium chromate, $BaCrO_4$ (also called Hashemite), is a naturally occurring chromate analogue of Barite. It has often been used as an oxidizing agent and as a catalyst for enhancing vapor-phase oxidation reactions.[39] Moreover, due to its excellent photophysical and photocatalytic properties, barium chromate is a highly efficient photocatalyst, with a particularly marked response to visible light irradiation.[40]

Recently, remarkable progress has been achieved, regarding the preparation of low-dimensional nanoscale metal tungstate, chromate, and sulfate derivatives. The synthesis of ordered microarrays of nanocrystals of both barium chromate and sulfate, with controlled chemical composition and size distribution, was reported using a reversed micelle templating method.[41] This methodology was subsequently extended to generate barium tungstate nanorods; the 2-dimensional organization of these $BaWO_4$ and $BaCrO_4$ nanorods at the water−air interface was accomplished using a Langmuir−Blodgett technique.[23,42] Recently, high aspect-ratio, single-crystalline $BaWO_4$ and $BaCrO_4$ nanowires with diameters as small as 3.5 nm and lengths up to more than 50 microns were synthesized in catanionic reverse micelles formed by an equimolar mixture of two surfactants: undecylic acid and decylamine.[43,44] With the further use of double-hydrophilic block copolymers as effective crystal growth modifiers, morphological variants, namely penniform $BaWO_4$ nanostructures, could be prepared using this technique.[45] Using an analogous idea, different $BaCrO_4$ nanostructures have been processed through a polymer-directed synthesis.[46−48] However, the development of facile, mild, and effective approaches for creating size-controlled 1-D nanostructures and their associated novel architectures remains a significant scientific challenge.

In this work, we have used a modified template synthesis technique, originally developed for the synthesis of organic microtubules, to successfully prepare free-standing single-crystalline $BaWO_4$ and $BaCrO_4$ nanorods and their arrays by physically placing two different precursor solutions in two halves of a U-tube cell, respectively, separated by alumina template membranes.[49,50] In other words, we use the pores in alumina membranes as the environment in which to control the growth of well-defined morphologies of single crystals of our ABO_4 nanostructures. The membranes used are thin, and are mounted in a double-diffusion setup, which enables the continuous flow of ions into the membrane pores and thus, the production of single crystals of ABO_4 nanocrystalline materials.

What is significant is that most nanostructures previously produced by conventional templating procedures are polycrystalline,[1] despite the variety of different deposition strategies used,

(22) Qi, L.; Ma, J.; Cheng, H.; Zhao, Z. *J. Phys. Chem. B* **1997**, *101*, 3460.
(23) Kwan, S.; Kim, F.; Akana, J.; Yang, P. *Chem. Commun.* **2001**, *(5)*, 447.
(24) Krumeich, F.; Muhr, H.-J.; Niederberger, M.; Bieri, F.; Schnyder, B.; Nesper, R. *J. Am. Chem. Soc.* **1999**, *121*, 8324.
(25) Wang, W.; Zhan, Y.; Wang, G. *Chem. Commun.* **2001**, *(8)*, 727.
(26) Liao, H.-W.; Wang, Y.-F.; Liu, X.-M.; Li, Y.-D.; Qian, Y.-T. *Chem. Mater.* **2000**, *12*, 2819.
(27) Martin, C. R. *Science* **1994**, *266*, 1961.
(28) Martin, C. R. *Chem. Mater.* **1996**, *8*, 1739.
(29) Lakshmi, B. B.; Dorhout, P. K.; Martin, C. R. *Chem. Mater.* **1997**, *9*, 857.
(30) Limmer, S. J.; Seraji, S.; Wu, Y.; Chou, T. P.; Nguyen, C.; Cao, G. Z. *Adv. Funct. Mater.* **2002**, *12*, 59.
(31) Schmid, G. *J. Mater. Chem.* **2002**, *12*, 1231.
(32) Mallouk, T. E. *Science* **2001**, *291*, 443.
(33) Hulteen, J. C.; Martin, C. R. *J. Mater. Chem.* **1997**, *7*, 1075.
(34) Yu, S.-H.; Liu, B.; Mo, M.-S.; Huang, J.-H.; Liu, X.-M.; Qian, Y.-T. *Adv. Funct. Mater.* **2003**, *13*, 639.
(35) Hu, X.-L.; Zhu, Y.-J. *Langmuir* **2004**, *20*, 1521.
(36) Cerny, P.; Zverev, P. G.; Jelinkova, H.; Basiev, T. T. *Opt. Commun.* **2000**, *177*, 397.
(37) Cerny, P.; Jelinkova, H. *Opt. Lett.* **2002**, *27*, 360.
(38) Nikl, M.; Bohacek, P.; Mihokova, E.; Kobayashi, M.; Ishii, M.; Usuki, Y.; Babin, V.; Stolovich, A.; Zazubovich, S.; Bacci, M. *J. Lumin.* **2000**, *87−89*, 1136.
(39) Economy, J.; Meloon Jr., D. T.; Ostrozynski, R. L. *J. Catal.* **1965**, *4*, 446.
(40) Yin, J.; Zou, Z.; Ye, J. *Chem. Phys. Lett.* **2003**, *378*, 24.
(41) Li, M.; Schnablegger, H.; Mann, S. *Nature* **1999**, *402*, 393.
(42) Kim, F.; Kwan, S.; Akana, J.; Yang, P. *J. Am. Chem. Soc.* **2001**, *123*, 4360.
(43) Shi, H.; Qi, L.; Ma, J.; Cheng, H.; Zhu, B. *Adv. Mater.* **2003**, *15*, 1647.
(44) Shi, H.; Qi, L.; Ma, J.; Cheng, H. *Chem. Commun.* **2002**, *(16)*, 1704.
(45) Shi, H.; Qi, L.; Ma, J.; Cheng, H. *J. Am. Chem. Soc.* **2003**, *125*, 3450.
(46) Yu, S.-H.; Antonietti, M.; Colfen, H.; Hartmann, J. *Nano Lett.* **2003**, *3*, 379.
(47) Yu, S.-H.; Colfen, H.; Antonietti, M. *Chem. Eur. J.* **2002**, *8*, 2937.
(48) Yu, S.-H.; Colfen, H.; Antonietti, M. *Adv. Mater.* **2003**, *15*, 133.
(49) Martin, C. R.; Van Dyke, L. S.; Cai, Z.; Liang, W. *J. Am. Chem. Soc.* **1990**, *112*, 8976.
(50) Liang, W.; Martin, C. R. *Chem. Mater.* **1991**, *3*, 390.

including electrochemical deposition, electroless deposition, polymerization, sol−gel deposition, and layer-by-layer deposition in nanoporous templates. The reason for the observed polycrystallinity is that many of these prior methodologies require additional annealing steps at high temperature.[29−31,33] By contrast, as we will discuss later, the formation mechanism of nanorods under our experimental conditions is analogous to a biomimetic crystallization process.[51] That is, the growth of our nanorods within the confinement of alumina membranes is analogous to the precipitation of single crystals of calcium carbonate and calcium phosphate within the confinement offered by gels, micelles, chitin scaffolds, and collagen matrixes.[52−55] Hence, nucleation and growth of single-crystalline nanomaterials occur essentially instantaneously through the direct chemical interaction between ions of the two different precursor solutions in contact with each other. The membrane acts to spatially direct crystal growth.

Moreover, at the same time, our simplistic technique allows for the reproducible fabrication of ordered, monodisperse 3-D arrays of these 1-D nanomaterials. This is critical, because assembly of nanoscale components (i.e., nanorods) is a key step toward building functional devices,[56] important for applications including nanoscale electronics and molecular sensing. Specifically, the fabrication of 3D arrays of 1-D nanomaterials, such as nanorods, is useful for optoelectronic applications, such as room-temperature ultraviolet lasing.[57] Though a number of preparative methods have been reported for generating these types of nanoscale architectures,[57−61] none of these techniques appears to work for ABO_4-type compound systems, with the exception of the current work. Furthermore, although we primarily focus on isolated 100 and 200 nm-sized $BaWO_4$ and $BaCrO_4$ nanorods and their associated arrays, we have noted that we can reproducibly form different sizes of these various nanoscale architectures using alumina template membranes of varying pore sizes.

Experimental Section

Materials Preparation. Alumina template membranes (Fisher Scientific) with pore sizes of 100 and 200 nm were prepared by a two-step aluminum anodic oxidation process.[31,33] The membrane was initially hydrated by immersion and sonication in a small volume of distilled, deionized water for a few minutes, so as to avoid air bubble formation within its structure or on its surface. Subsequently, the membrane was mounted between the two halves of a U-tube cell. The half-cells were then filled with equimolar solutions of $Ba(NO_3)_2$ and either Na_2WO_4 or Na_2CrO_4 solutions to generate barium tungstate and barium chromate, respectively. After immersion times of up to 12 h at room temperature, the alumina template, into which the precursors had presumably diffused resulting in product formation, was detached and thoroughly washed with deionized water. The alumina membrane was subsequently dissolved by immersion in 1 M NaOH for about 30 min. Figure 1 schematically illustrates the experimental setup utilized.

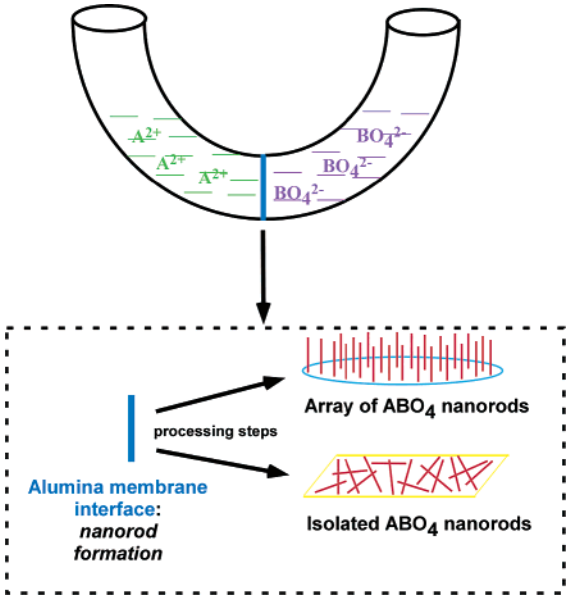

Figure 1. Schematic of setup used to synthesize ABO_4 nanostructures, such as $BaWO_4$ and $BaCrO_4$ nanorods.

The nanorods, which were characterized by means of X-ray diffraction (XRD), scanning electron microscopy (SEM), transmission electron microscopy (TEM), high resolution TEM (HRTEM), selected area electron diffraction (SAED), energy-dispersive X-ray spectroscopy (EDS), Raman and FT-IR analyses, were collected by centrifugation. These were then washed with deionized water until the pH of the product suspensions attained approximately a value of 7. To prepare SEM samples of the corresponding $BaWO_4$ and $BaCrO_4$ nanorod arrays, a previously developed procedure was utilized.[29] Briefly, alumina membranes containing $BaWO_4$ and $BaCrO_4$ nanorods were glued (using Epoxy resin) to a piece of paper towel. Resulting composites were immersed into a 1 M NaOH aqueous solution for ~0.5 h to dissolve the alumina. After washing steps with distilled, deionized water followed by air-drying, samples were subsequently mounted onto SEM stubs for imaging.

Materials Characterization. Products were characterized by a number of different methodologies, including XRD, SEM, TEM, HRTEM, SAED, and EDS as well as with Raman and FT-IR spectroscopies.

X-ray Diffraction. Crystallographic and purity information on the as-prepared barium tungstate and barium chromate nanostructure samples were obtained using powder XRD. To generate these samples, the as-prepared $BaWO_4$ and $BaCrO_4$ products, upon centrifugation, were subsequently sonicated for about 1 min, and later air-dried upon deposition onto glass slides. The diffraction patterns were collected using a Scintag diffractometer, operating in the Bragg configuration using Cu K_α radiation ($\lambda = 1.54$ Å) from 10 to 80° at a scanning rate of 2° per minute.

Electron Microscopy. The size and morphology of the resulting $BaWO_4$ and $BaCrO_4$ products were initially characterized using a field emission SEM (FE-SEM Leo 1550) at accelerating voltages of 15 kV. Specifically, solid $BaWO_4$ and $BaCrO_4$ samples of isolated nanorods and their associated arrays immobilized onto Epoxy resin were mounted onto conductive carbon tapes, which were attached to the surfaces of SEM brass stubs. These samples were then conductively coated with gold by sputtering for 15 s to minimize charging effects under SEM imaging.

Low magnification TEM images were taken at an accelerating voltage of 120 kV on a Philip CM12 instrument, equipped with EDS

(51) Dorozhkin, S. V.; Dorozhkina, E. I.; Epple, M. *Cryst. Growth Des.* **2004**, *4*, 389.
(52) Becker, A.; Becker, W.; Marxen, J. C.; Epple, M. *Z. Anorg. Allg. Chem.* **2003**, *629*, 2305.
(53) Grassmann, O.; Lobmann, P. *Biomaterials* **2004**, *25*, 277.
(54) Schwarz, K.; Epple, M. *Chem. Eur. J.* **1998**, *4*, 1898.
(55) Falini, G.; Fermani, S.; Ripamonti, A. *J. Inorg. Biochem.* **2002**, *91*, 475.
(56) Colfen, H.; Mann, S. *Angew. Chem., Int. Ed.* **2003**, *42*, 2350.
(57) Huang, M. H.; Mao, S.; Feick, H.; Yan, H.; Wu, Y.; Kind, H.; Weber, E.; Russo, R.; Yang, P. *Science* **2001**, *292*, 1897.
(58) Yang, P. *Nature* **2003**, *425*, 243.
(59) Feng, X.; Feng, L.; Jin, M.; Zhai, J.; Jiang, L.; Zhu, D. *J. Am. Chem. Soc.* **2004**, *126*, 62.
(60) Tian, Z. R.; Voigt, J. A.; Liu, J.; McKenzie, B.; Mcdermott, M. J.; Rodriguez, M. A.; Konishi, H.; Xu, H. *Nat. Mater.* **2003**, *2*, 821.
(61) Tian, Z. R.; Voigt, J. A.; Liu, J.; McKenzie, B.; Xu, H. *J. Am. Chem. Soc.* **2003**, *125*, 12384.

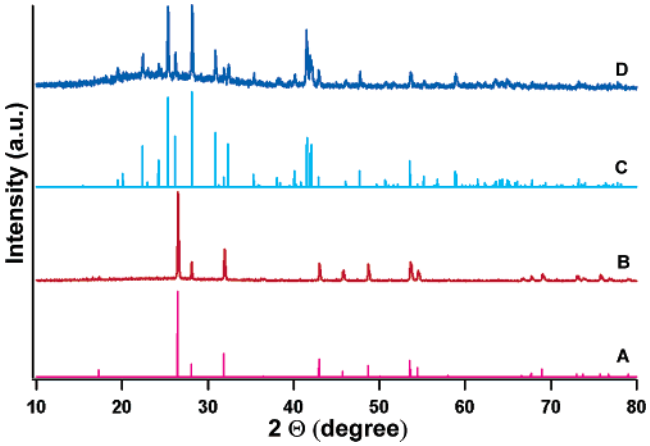

Figure 2. XRD patterns arising from (A) JCPDS no. 72-0746 database standard ($BaWO_4$); (B) as-prepared $BaWO_4$ nanorod sample; (C) JCPDS no. 78-1401 database standard ($BaCrO_4$); and (D) as-prepared $BaCrO_4$ nanorod sample.

capabilities. HRTEM images and SAED patterns as well as EDS data were obtained on a JEOL 2010F HRTEM (equipped with an Oxford INCA EDS system and subsequent potential of performing SAED) at an accelerating voltage of 200 kV to further characterize individual $BaWO_4$ and $BaCrO_4$ nanorods. Specimens for all of these TEM studies were prepared by depositing a drop of these aqueous suspension samples onto a 300 mesh Cu grid, coated with a lacey carbon film. Prior to deposition, solutions containing samples of $BaWO_4$ and $BaCrO_4$ nanorods, were sonicated for 2 min to ensure adequate dispersion of the nanorods.

Optical Spectroscopy. Samples for Raman spectroscopy were analyzed on a Kaiser micro-Raman instrument, with a 200-micron confocal aperture, at a laser excitation of 752.5 nm using a power level of 5 mW. Infrared spectra were obtained, using a ThermoNicolet Nexus 670 using a ZnSe single reflectance ATR accessory.

Results and Discussion

X-ray Diffraction. As-prepared $BaWO_4$ and $BaCrO_4$ nanorod samples were examined by powder XRD measurements on a Scintag diffractometer with Cu Kα radiation (Figure 2). Diffraction peaks in Figure 2B can be indexed to a scheelite-structured, tetragonal phase $BaWO_4$ with calculated cell constants of $a = 5.610$ Å and $c = 12.711$ Å, which are numerically close to the reported values of the bulk materials (Figure 2A, JCPDS File No. 72-0746). By analogy, diffraction peaks in Figure 2D can be indexed to a hashemite-structured, orthorhombic phase $BaCrO_4$ with calculated cell constants of $a = 9.105$ Å, $b = 5.541$ Å, and $c = 7.343$ Å, which are consistent with the literature data (Figure 2C, JCPDS File No. 78-1401).

Electron Microscopy. The morphology of the as-synthesized $BaWO_4$ and $BaCrO_4$ nanorod samples was obtained using FE-SEM and low magnification TEM. Typical SEM and TEM images of $BaWO_4$ nanorods are depicted in Figure 3A and 3B, respectively. On the basis of these data, it can be observed that straight, smooth, and crystalline wire-like $BaWO_4$ nanorods, with a uniform diameter throughout their entire length, were produced. Diameters of $BaWO_4$ nanorods obtained were ~200 ± 25 nm (25 different nanorods), based on the 200 nm pore sizes of the alumina membranes used in the synthesis. The shapes of these nanorods clearly replicated the pore structure of the corresponding alumina templates. The lengths of the $BaWO_4$ nanorods were as much as several microns.

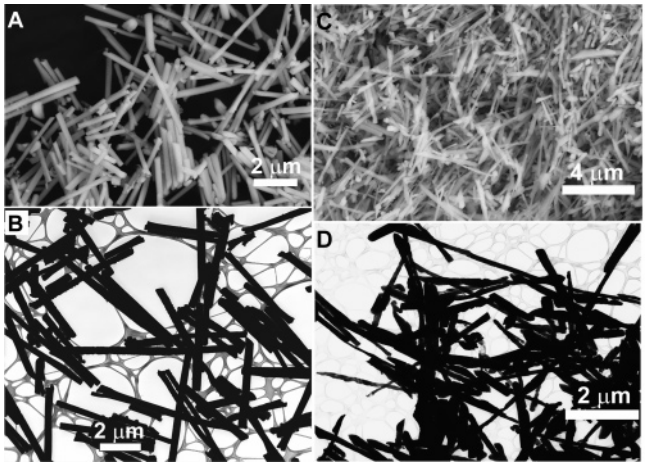

Figure 3. (A) Typical SEM micrograph of $BaWO_4$ nanorods. (B) Representative TEM image of $BaWO_4$ nanorods. (C) Typical SEM micrograph of $BaCrO_4$ nanorods. (D) Representative TEM image of $BaCrO_4$ nanorods.

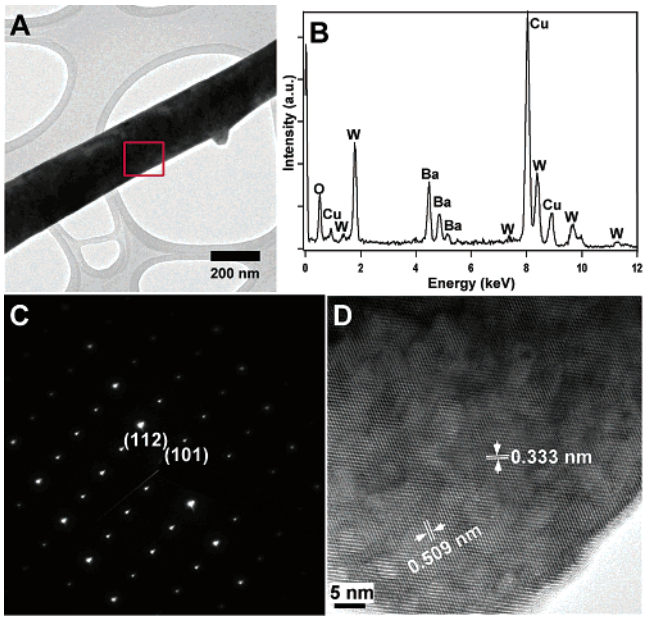

Figure 4. (A) TEM image of a single $BaWO_4$ nanorod. (B) EDS of as-prepared $BaWO_4$ nanorods. The Cu peaks originate from the TEM grid. SAED pattern (C) and HRTEM image (D) of a representative portion of a $BaWO_4$ nanorod, as delineated by the red square, in (A).

Figure 3, parts C and D, shows representative SEM and TEM images of $BaCrO_4$ nanorods, respectively. It can be observed that smooth and crystalline wire-like $BaCrO_4$ nanorods were produced. Diameters of the $BaCrO_4$ nanorods obtained were in the range of 100 ± 15 nm (25 different nanorods), based upon the 100 nm pore size of the alumina membranes used as the templates. $BaCrO_4$ nanorods synthesized reached an aspect ratio of up to 15.

To provide further insight into the structure of the as-prepared $BaWO_4$ and $BaCrO_4$ nanostructures, individual nanorods were analyzed by HRTEM as well as using SAED and EDS. An image of a randomly chosen single $BaWO_4$ nanorod is shown in Figure 4A. To confirm the chemical composition of the as-prepared nanorods, EDS spectra (Figure 4B) were recorded at a number of different positions along a single nanorod. The chemical signatures obtained are identical within experimental

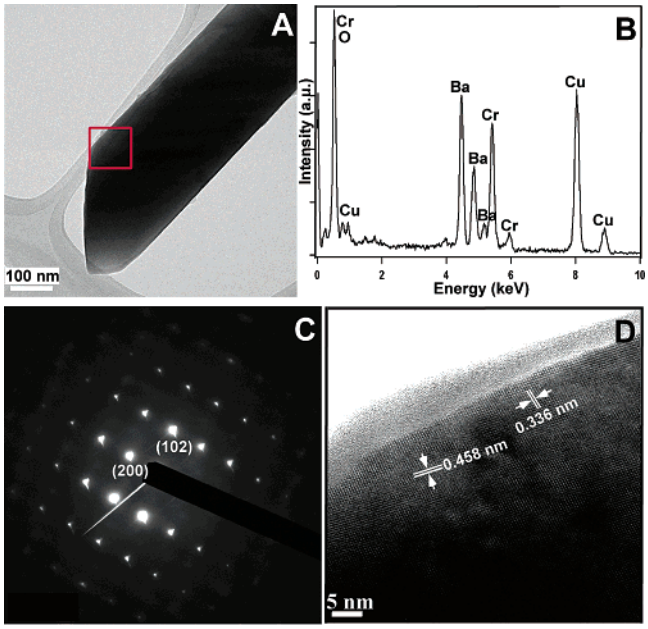

Figure 5. (A) TEM image of a single $BaCrO_4$ nanorod. (B) EDS of as-prepared $BaCrO_4$ nanorods. The Cu peaks originate from the TEM grid. SAED pattern (C) and HRTEM image (D) of a representative portion of a $BaCrO_4$ nanorod, as defined by the red square, in (A).

accuracy, and essentially only Ba, W, and O elements are observed from the nanorod structure. The Cu signal arises from the TEM grid.

Figure 4C presents the SAED pattern taken from a portion of a single $BaWO_4$ nanorod shown in Figure 4A. We note that the electron diffraction patterns obtained from different positions along individual nanorods are essentially identical within experimental accuracy (Figure S1). Whereas template methods typically yield polycrystalline nanostructures,[1] the presence of the sharp diffraction spots rather than an amorphous ring is suggestive of the predicted formation of single-crystalline $BaWO_4$. The associated electron diffraction pattern is consistent with pure $BaWO_4$ crystals of a tetragonal scheelite structure, indexed as shown in Figure 4C. In Figure 4D, a HRTEM image of a portion of an individual $BaWO_4$ nanorod, shown in Figure 4A, is displayed. While a thin amorphous layer likely coats the outer $BaWO_4$ nanorod surface, the HRTEM image further confirms that the observed $BaWO_4$ nanorods are single crystalline with no defects or dislocations. The 2-D lattice fringes reveal that the single-crystalline $BaWO_4$ nanorods possess interplanar spacings of about 5.09 and 3.33 Å, corresponding to the (101) and (112) planes, respectively.

Figure 5A presents an individual $BaCrO_4$ nanorod. EDS elemental analysis data (Figure 5B) confirm the presence of Ba, Cr, and O elemental signatures associated with the product in the expected stoichiometric proportions. The SAED pattern taken from a single $BaCrO_4$ nanorod (Figure 5C and Figure S2) yields sharp diffraction spots rather than rings, which are suggestive of the presence of single-crystalline $BaCrO_4$. The related electron diffraction pattern is consistent with pure $BaCrO_4$ crystals of an orthorhombic hashemite structure, indexed as shown in Figure 5C. Figure 5D presents a HRTEM image of a portion of an individual $BaCrO_4$ nanorod, initially described in Figure 5A. This image reveals that the $BaCrO_4$ nanorod is single-crystalline with lattice fringe spacings of ~4.58 and 3.36 Å, respectively. These two planes can be indexed as the {200} and {102} planes, respectively, of an orthorhombic-phase $BaCrO_4$ crystal (JCPDS card no. 78-1401).

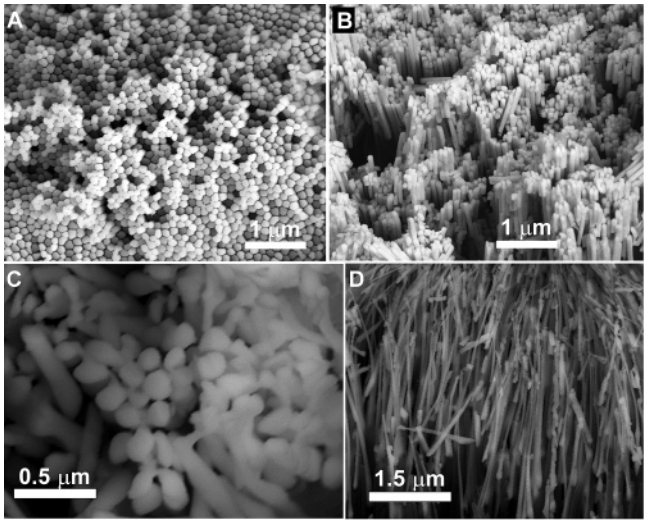

Figure 6. SEM images of as-prepared $BaWO_4$ nanorod arrays: (A) top-view; (B) tilt-view. Analogous images of as-prepared $BaCrO_4$ nanorod arrays: (C) top-view; (D) tilt-view. The less-than-optimal packing of $BaCrO_4$ nanomaterials arises from the inhomogeneous distribution of the as-formed individual nanorods.

Figure 6 illustrates the top and tilt views of the SEM images of $BaWO_4$ and $BaCrO_4$ nanorod arrays, respectively, grown within the alumina templates. The SEMs show that the nanorods are individually separated from each other. Nonetheless, they form a dense, continuous network, where the nanorods are roughly parallel to each other and vertically oriented on the substrates to form a packed array, stretching over micron-sized areas. This is especially true of $BaWO_4$. The diameters of these nanorods are about 101 ± 8 nm (50 different nanorods), corresponding to the diameter of channels in the alumina template. What is important to note is that these arrays of ABO_4-type nanorods were produced very readily at room temperature without the need for sophisticated experimental setups[57] (characteristic of arrays formed by vapor transport via VLS-type methodologies), or for high-temperature annealing (associated with sol−gel template approaches).[29,30,33] Moreover, the sizes of these $BaWO_4$ and $BaCrO_4$ nanorods could be readily varied by choosing membranes, possessing different pore sizes.

To investigate the thermal stability of the as-prepared nanorods, samples of $BaWO_4$ and $BaCrO_4$ nanorods were further heated in air for 5 h at 650 °C. Figure 7 reveals that their morphologies and crystallographic orientations remain essentially unaltered after this annealing step. It is noteworthy that the thickness of the surface amorphous layer on the nanorods is somewhat thinner than that of the as-prepared samples. Hence, samples of $BaWO_4$ and $BaCrO_4$ nanorods should be suitable for applications at elevated temperatures, such as high-temperature catalysis.

Optical Spectroscopy. Optical properties of our synthesized nanorods were also investigated. Figure 8 shows Raman spectra of the as-prepared products and the corresponding bulk commercially available samples (Aldrich) of $BaWO_4$ and $BaCrO_4$, corroborating the chemical identity of our nanostructures. Spectra of the as-prepared nanorods (Figure 8B and 8D) show typical Raman bands, which can be attributed to crystalline

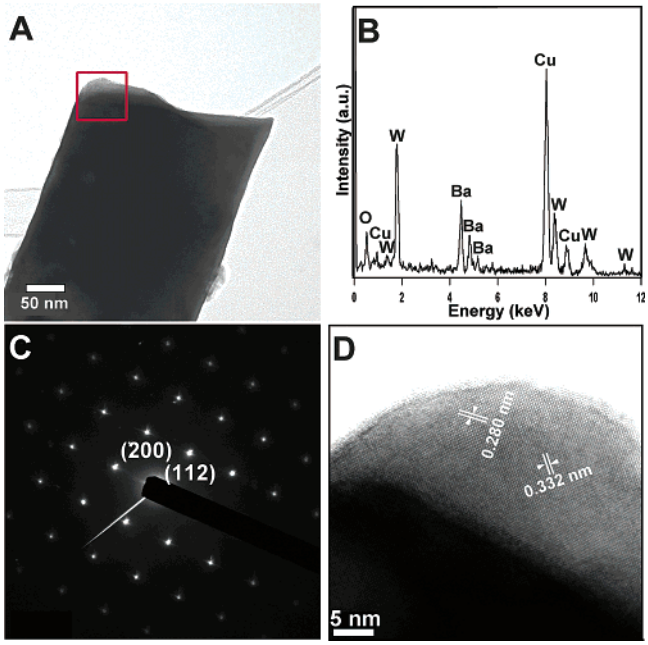

Figure 7. $BaWO_4$ nanorods upon annealing in air for 5 h at 650 °C. (A) TEM image of a single $BaWO_4$ nanorod. (B) EDS of the $BaWO_4$ nanorod, shown in (A). Cu peaks originate from the TEM grid. SAED pattern (C) and HRTEM image (D) from a portion of a $BaWO_4$ nanorod, as delineated by the red square in (A).

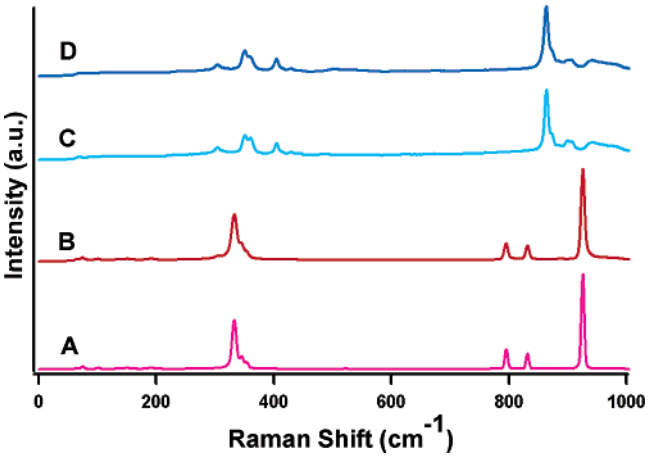

Figure 8. Raman spectra of (A) bulk commercial, crystalline $BaWO_4$ powder; (B) as-prepared single-crystalline $BaWO_4$ nanorods; (C) bulk commercial, crystalline $BaCrO_4$ powder; and (D) as-prepared single-crystalline $BaCrO_4$ nanorods.

$BaWO_4$ and $BaCrO_4$, respectively.[62,63] According to the reported literature, the vibrational modes of isolated BO_4 tetrahedra can be separated into internal, external translational, and rotational modes. As shown in Figure 8B, bands at 927, 833, 797, 347, and 334 cm^{-1} can be assigned to the $\upsilon_1(A_g)$, $\upsilon_3(B_g)$, $\upsilon_3(E_g)$, $\upsilon_4(B_g)$, and $\upsilon_2(B_g)$ modes, respectively, of the as-prepared $BaWO_4$ nanorods. Peaks located at 197 and 159 cm^{-1}, as well as at 106 and 78 cm^{-1}, can also be assigned to their rotational (A_g, E_g) and translational modes (E_g, B_g), respectively. In Figure 8D, peaks at positions corresponding to 909/906, 864, 432/406, and 361/352 cm^{-1} could be attributed to the υ_3, A_g, υ_4, and υ_2 modes, respectively, of as-prepared $BaCrO_4$ nanorods. Moreover, bands at 306 and 72 cm^{-1} can be assigned to the lattice vibrations of $BaCrO_4$ nanorods.

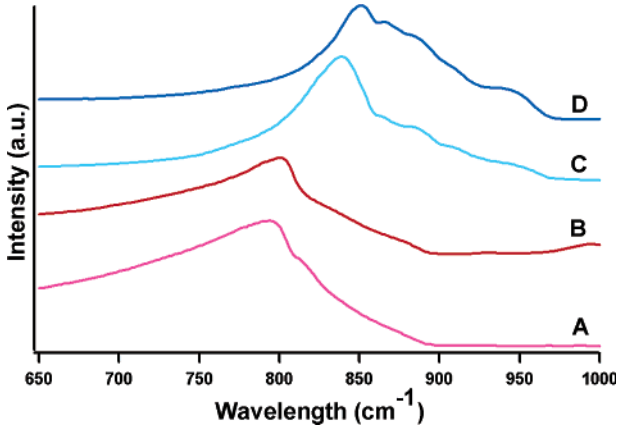

Figure 9. FT-IR spectra of (A) bulk commercial, crystalline $BaWO_4$ powder; (B) as-prepared single-crystalline $BaWO_4$ nanorods; (C) bulk commercial, crystalline $BaCrO_4$ powder; and (D) as-prepared single-crystalline $BaCrO_4$ nanorods.

In the FT-IR spectra (Figure 9), the strong band at 802 cm^{-1} and its shoulder (Figure 9B) appear to result from the E_u and A_u components, respectively, of the υ_3 band of $BaWO_4$ nanorod sample. In addition, one υ_1 band at 852 cm^{-1} and three additional υ_3 bands at 868, 885, and 943 cm^{-1}, respectively, have been observed, associated with the $BaCrO_4$ nanorod sample (Figure 9D).[62,63]

Considering the imperfect correlation between the IR spectra of the bulk solid (Figure 9A, C) vs nanorod samples (Figure 9B, D), it turns out that this type of phenomenon has been observed previously. First of all, in tungstate and molybdate systems,[62] for some of the IR-active vibrations, the frequency difference between the longitudinal optic and the transversal optic modes is rather large, and the location of the 'absorption' maximum of these samples often depends on the granular nature of the sample. Indeed, for the high-frequency band at around 820 cm^{-1}, the situation is further complicated by the overlapping in the same spectral region of 2 IR-active components of υ_3. Second, there is a larger degree of surface strain, associated with the smaller nanocrystal; this effect may be related to changes in coupling to lattice vibrational modes. Third, the blue shift in the infrared absorption peaks of our chromate and tungstate nanocrystals as compared with their bulk counterparts may be attributed to quantum confinement effects. Similar behavioral trends have been observed for a number of other systems including $CaCO_3$, InSb, and VO_2.[64−67]

The results of Raman and IR data further corroborate the other data collected, confirming the identity of our as-prepared nanomaterials as indeed $BaWO_4$ and $BaCrO_4$, respectively. The generation of these materials provides the basis for a more thorough future investigation of their novel optical, optoelectronic, and catalytic properties for possible incorporation into nanoscale devices. We believe that the lasing and photocatalytic properties of these materials will be particularly intriguing.

(62) Miller, P. J.; Khanna, R. K.; Lippincott, E. R. *J. Phys. Chem. Solids* **1973**, *34*, 533.
(63) Scheuermann, W.; Schutte, C. J. H. *J. Raman Spectrosc.* **1973**, *1*, 605.
(64) Zhu, K.; Shi, J.; Zhang, L. *Solid State Commun.* **1998**, *107*, 79.
(65) Tarte, P.; Liegeois-Duyckaerts, M. *Spectrochim. Acta* **1972**, *28A*, 2029.
(66) Yue, L.-H.; Shui, M.; Xu, Z.-D. *J. Zhejiang Uni., Sci.* **2000**, *1*, 178.
(67) Zheng, C.; Zhang, X.; Zhang, J.; Liao, K. *J. Solid State Chem.* **2001**, *156*, 274.

Plausible Formation Mechanism

As described previously, in the current study, we use the pores of alumina membranes as the physical environment in which to control the growth of well-defined morphologies of single crystals of our ABO_4 structures. The membranes used are thin, and are mounted in a double-diffusion setup, which enables the continuous flow of ions into the membrane pores and thus, the production of single crystals of ABO_4 nanocrystalline materials. Based on our experimental results, we propose that single crystals of nanoscale ABO_4 materials derive from isolated, disparate nucleation sites (consisting of ABO_4 nuclei generated via the reaction between A^{2+} and BO_4^{2-}), which then grow by extension through the porous network. Continued growth then occurs at the particle surface at a rate limited by ion availability, until the crystal impinges on the alumina template surface, which ultimately limits further growth. Hence, by the spatially constrained volume defined by the presence of the template itself (Figure S3), nanorods instead of nanoparticles are formed due to the growth environment conducive to these 1-dimensional structures.

We note that we are not forming hollow nanotubes because the interactions between the reagent molecules are likely stronger than those between the reagent molecules and the pore walls. In the case of polymeric microtubules formed in templates, nascent polymer chains initially adsorb to the pore walls yielding a thin polymer 'skin', that becomes thicker with time until quenching with water.[49] We do not believe this image accurately reflects the growth mechanism of our system, which is effectively akin to biomineralization.

In the current study, the growth mechanism involves a double diffusion crystallization setup process,[68−70] comprising two reservoirs of solutions that each contains a part of an insoluble salt (ABO_4), i.e., A^{2+} on one side and BO_4^{2-} on the other side. To prevent overly rapid mixing, the solutions are separated by an alumina membrane that slows down diffusion and rate of crystallization. However, when the two solutions do meet, precipitation occurs, depleting the availability of ions in the local environment of the growing crystal within the template. The fact that single nanorods can grow is suggestive of the fact that nucleation within the membrane itself is likely limited, an effect promoted by the relatively inert surface of the membrane. The nucleation rate is primarily dictated by the supersaturation of the solution. Further growth of the nanorods is limited by diffusion of ions in this localized region.

The shape of the alumina membranes has a crucial effect on the morphology of the ABO_4 phase that subsequently forms. In fact, we note instances where the morphology of the ABO_4 nanorods spatially maps out the interior nanoscopic profile and localized contours of the internal pores of the alumina membranes. That is, whereas the majority of as-prepared $BaWO_4$ and $BaCrO_4$ nanorods were straight and possessed smooth surfaces, a small number of $BaWO_4$ and $BaCrO_4$ nanorods with protrusions or depressions on their surfaces were also produced, reflecting the morphology and inner surface roughness of the pores from whence they were formed. Figures 10A and 10D show examples of a hump-like protrusion from an ~200 nm $BaWO_4$ nanorod as well as a pit-like depression from an ~100 nm $BaCrO_4$ nanorod, respectively, likely arising from imperfections within the alumina pores. It was evident that even in these regions, the nanorods remained pure and single-crystalline, clearly preserving their 2-D lattice fringes (i.e., Figure 10B, C, and E).

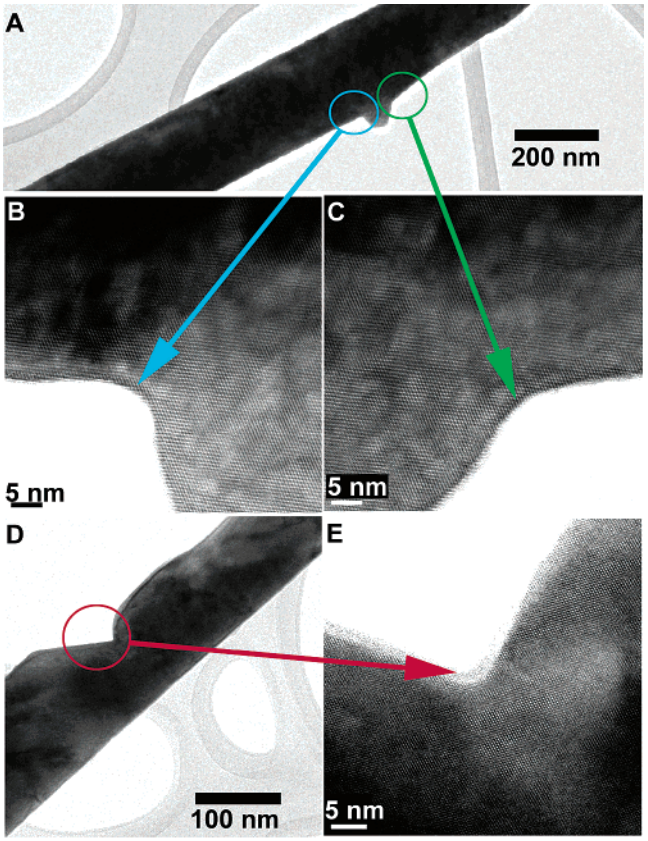

Figure 10. (A) TEM image of a single $BaWO_4$ nanorod containing a protrusion. (B and C) HRTEM images corresponding to different sections, defined by the blue and green circles, respectively, of the single $BaWO_4$ nanorod, shown in (A). (D) TEM image of a single $BaCrO_4$ nanorod containing a notched depression. (E) HRTEM view of the portion of the single $BaCrO_4$ nanorod, highlighted by a red circle in (D).

Conclusions

The current work demonstrates the room-temperature preparation using a novel, modified template-assisted methodology of single-crystalline $BaWO_4$ nanorods and $BaCrO_4$ nanorods with different controllable sizes as well as the creation of arrays of these nanorods in the pores of an alumina membrane at room temperature. The resulting nanorods and the arrays have been extensively characterized using a variety of microscopy and spectroscopy results. Because of the simplicity and generalizability of the approach used, it is anticipated that this methodology can be generalized to the synthesis of other important tungstate, molybdate, chromate, sulfate, iodate, and selenate systems at the nanoscale, such as $SrWO_4$, $BaMoO_4$, $ZnWO_4$, $BaSO_4$, and $BaIO_4$ as well as $Ba_{1-x}Sr_xWO_4$. Moreover, we can likely prepare single-crystalline nanorods of smaller diameters (to a certain extent) using smaller diameter templates.

In addition, due to the ease of preparation and the thermal stability of the nanorods that are now available, our newly established synthetic method could become a valuable starting point for generating functional nanoscale devices. In particular, creation of arrays of nanorods presents an interesting illustration

(68) Park, R. J.; Meldrum, F. C. *Adv. Mater.* **2002**, *14*, 1167.
(69) Park, R. J.; Meldrum, F. C. *J. Mater. Chem.* **2004**, *14*, 2291.
(70) Peters, F.; Epple, M. *J. Chem. Soc., Dalton Trans.* **2001**, *(24)*, 3585.

of the idea of bottom-up assembly using nanoscale building blocks. Future research will focus on more extensive investigations of the physical (e.g., optoelectronic and photocatalytic) properties of individual nanorods and nanorod arrays.

Acknowledgment. We acknowledge support of this work through startup funds provided by the State University of New York at Stony Brook as well as Brookhaven National Laboratory. In addition, research was supported in part by the U.S. Department of Energy Office of Basic Energy Sciences under Contract DE-AC02-98CH10886. Acknowledgment is also made to the National Science Foundation for a CAREER award (DMR-0348239), and the donors of the Petroleum Research Fund administered by the American Chemical Society, for support of this research. Y.M. recognizes Sigma Xi for a Grant-in-Aid of Research. S.S.W. thanks 3M for a nontenured faculty award. We also thank Professor Jianyu Huang (Physics Department, Boston College) and Dr. James Quinn (Materials Science Department, SUNY at Stony Brook) for their help with HRTEM and SEM/TEM analyses, respectively. The assistance of Dr. Alasdair Bell and of the late Mr. Rudolph Schlott (Chemistry Department, SUNY at Stony Brook) with Raman analyses and U-tube glass fabrication, respectively, has been appreciated. Sarbajit Banerjee and Tirandai Hemraj-Benny (Chemistry Department, SUNY at Stony Brook) are acknowledged for their help with the FT-IR analysis.

Supporting Information Available: Additional selected area electron diffraction patterns are presented, associated with Figures 4 and 5 of the main text. A SEM image of the cross-section of a 200 nm pore-sized alumina template, containing $BaWO_4$ nanorods is also shown. This material is available free of charge via the Internet at http://pubs.acs.org.

JA046331J